ACS OMEGA

http://pubs.acs.org/journal/acsodf

Article

Solventless Preparation of Thoria and Its Inclusion into SiO_2 and TiO_2: A Luminescence and Photocatalysis Study

Carlos Diaz,* M. L. Valenzuela,* Miguel A. Laguna-Bercero, Daniel Carrillo, Marjorie Segovia, Karina. Mendoza, and Patricio Cartes

Cite This: *ACS Omega* 2021, 6, 9391−9400

Read Online

ACCESS | Metrics & More | Article Recommendations | Supporting Information

ABSTRACT: Thoria was prepared using a solid-state method from the macromolecular precursor Chitosan·$Th(NO_3)_4$ (chitosan) and PS-co-4-PVP·$Th(NO_3)_4$ (PVP). The morphology and the average size of ThO_2 depend of the chitosan and PS-co-4-PVP polymer forming the precursor. Their photoluminescent properties were investigated, finding a dependence of their intensity emission maxima, with the nature of the precursor polymer. The photocatalytic activity of ThO_2 toward the degradation of methylene blue was measured for the first time, finding a degradation of about 66% in 300 min. The inclusion of ThO_2 into SiO_2 and TiO_2 was achieved by the solid-state pyrolysis of the macromolecular composites Chitosan·$Th(NO_3)_4$//MO_2 and PS-co-4-PVP·$Th(NO_3)_4$//MO_2, MO_2 = SiO_2 or TiO_2. The ThO_2 exhibits a homogeneous dispersion inside the silica, showing sizes of about 40 and 50 nm for the chitosan and PVP polymer precursors, respectively. The luminescent properties of the ThO_2/SiO_2 and ThO_2/TiO_2 composites were also studied, finding a decrease in intensity when introducing the SiO_2 or TiO_2 matrices. The photocatalytic behavior to methylene blue degradation of ThO_2 and their composites ThO_2/SiO_2 and ThO_2/TiO_2 was investigated for the first time, with them in the following order: ThO_2 > ThO_2/TiO_2 > ThO_2/SiO_2.

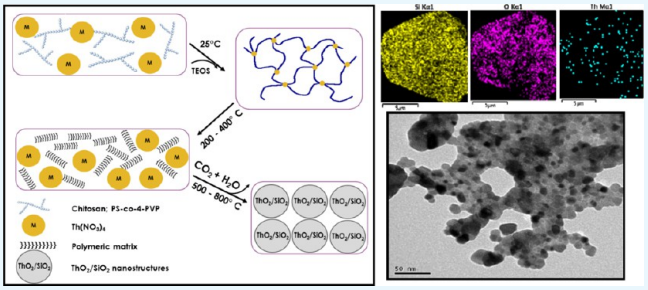

INTRODUCTION

Among actinides oxides, thoria is an important and promising material used in ceramic catalyst sensor solid electrolytes, catalysis and optical materials, and in the traditional nuclear industry.[1−4] In spite of this, few papers related to the preparation and properties of nanostructured ThO_2 have been reported. Among other methods, thermolysis, precipitation, sol−gel, or hydrothermal synthesis under supercritical conditions were proposed. Dash et al.[5] prepared ThO_2 by thermal decomposition of $Th(CO_3)_2$, while Tabakova[6] prepared thoria starting from $Th(NO_3)_4$ and then precipitating the thorium hydroxide with $K_2(CO_3)_2$ followed by thermal treatment. A similar route was followed by Reibold et al.,[7] preparing thoria by hydrolysis of $Th(NO_3)_4$ in the presence of ammonium hydroxide and propylene oxide. In another approximation, Moeini et al.[8] prepared ThO_2 by a hydrothermal process employing supercritical water. Most recently, Hudry et al.[3] used the oleyamine method to prepare ThO_2 of controlled morphology, while Shi and co-workers also prepared ThO_2 using a hydrothermal method starting from $Th(NO_3)_4$ pentahydrate.[9] Recently, Pinkas[10] reports the preparation of thorium dioxide with nanofibrous morphology by the electrospinning method. Also, Romanchuk[11] reported that the facile chemical precipitation method and subsequent thermal treatment were shown to be suitable for preparation of crystalline ThO_2 nanoparticles. Verma[12] has newly reported that ThO_2 nanoflowers can be successfully synthesized using thorium nitrate pentahydrate as the metal source along with two different capping agents.

Almost all of these preparation methods involve solution procedures. However, several of the abovementioned practical applications require the incorporation of ThO_2 into solid-state devices. Generally, the incorporation of metal-oxide nanoparticles into solid devices is problematic when those have been produced via a solution phase method because the solid-state isolation could cause nanoparticle agglomeration.[13−16] In this regard, the synthesis of nanoparticles directly from a solid-state approach might represent a more reliable method to achieve the incorporation of metal oxides into practical applications.

In addition, various practical applications—for instance, catalysis—involving solid-state devices are formed by nanoparticles and/or nanostructures inside a solid matrix, such as

Received: November 30, 2020
Accepted: March 19, 2021
Published: April 2, 2021

https://doi.org/10.1021/acsomega.0c05811
ACS Omega 2021, 6, 9391−9400

Scheme 1. Schematic Representation of the Preparation of the Composites ThO_2/SiO_2 and ThO_2/TiO_2

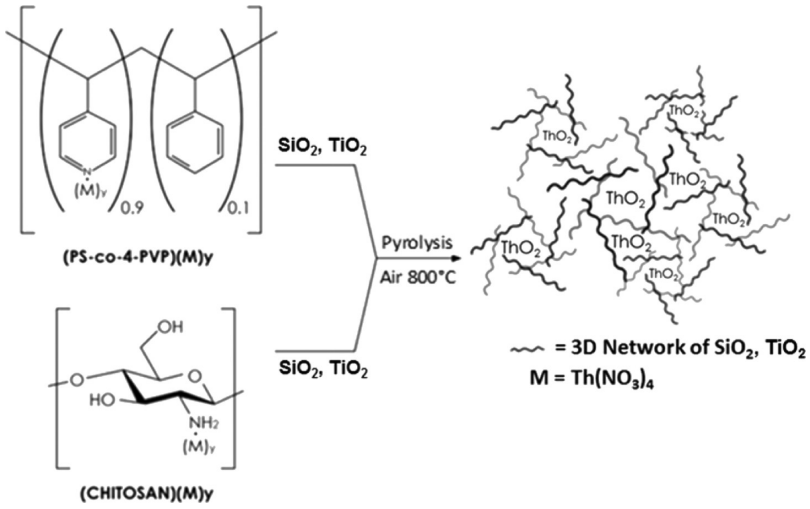

SiO_2, TiO_2, Al_2O_3, glasses, and so on.[17,18] For this reason, we will show results about the incorporation of thoria inside SiO_2 and TiO_2 matrices. This solid-state route synthesis method to prepare nanostructured metal and metal oxides materials from thermal treatment of the Chitosan·$(MLn)_n$ and PS-co-4-PVP·$(MLn)_n$ precursors under an air atmosphere was developed recently.[19−21]

In this paper, we have applied this methodology to prepare nanostructured ThO_2 from the chitosan and PVP precursors. We also present an easy alternative procedure to prepare nanostructured thoria and their inclusion inside SiO_2 and TiO_2, as seen in Scheme 1. Their photoluminescent properties and the photocatalytic activity toward the degradation of methylene blue were also investigated.

This novel and original work includes the first systematic study of the effect of different matrices—SiO_2 and TiO_2—in a metal oxide such as thoria, determining their optical and photocatalytic properties. There are very limited studies regarding ThO_2 photocatalytic activity and more especially regarding its combined effect with different matrices.

The inclusion of thoria will be performed by a novel solid-state thermolysis of different chitosan and PVP precursors, ensuring a regular distribution of thoria with the different Ti and Si oxides.

METHODOLOGY DESCRIPTION

Reagents. $Th(NO_3)_4$, TEOS (tetraethylortosilicate), chitosan, and poly(styrene-*co*-4-vinilpyridine) PS-co-4-PVP were purchased from Sigma-Aldrich and were used as-received.

Preparation: Synthesis of the Precursors. *Chitosan·$Th(NO_3)_4$ and PS-co-4-PVP·$Th(NO_3)_4$.* The typical procedure is described as follows: in a Schlenk flask, an appropriate amount of $Th(NO_3)_4$ and chitosan or PS-co-4-PVP were added into CH_2Cl_2 at different [polymer/$Th(NO_3)_4$] molar ratios (1:1; 1:5). The heterogeneous mixture was stirred at room temperature for a given reaction time (reaction time and additional details for each $Th(NO_3)_4$ reaction are explained in Table S1 of the Supporting Information). After removing the supernatant solution by decantation, the remaining solid was dried under reduced pressure to give a white solid.

Chitosan·$Th(NO_3)_4$//SiO_2 and PS-co-4-PVP·$Th(NO_3)_4$//SiO_2. SiO_2 was prepared according to the following literature procedure.[21] Briefly, tetraethoxysilane (TEOS), ethanol, and acetic acid in a molar ratio of 1:4:4 were mixed with water (nanopure), and the mixture was stirred for 3 days. The obtained gel was dried at 100 °C under reduced pressure in a vacuum furnace.

Pyrolysis of the Precursors. Pyrolysis experiments were performed using 0.05−0.15 g of the metallic Chitosan·$Th(NO_3)_4$ and PS-co-4-PVP·$Th(NO_3)_4$ precursors, as well as their composites with SiO_2. The samples were placed in alumina boats and heated in a furnace (Daihan oven model Wise Therm FHP-12) under an airflow up to 200 °C and then to 800 °C, followed by annealing for 2−4 h. The heating rate was fixed at 10 °C min^{-1} for all experiments.

Characterization of the Pyrolytic Products. The solid pyrolytic samples were characterized by X-ray powder diffraction (XRD), scanning electron microscopy (SEM), high-resolution transmission electron microscopy (HR-TEM), Fourier transform infrared (FT-IR) spectroscopy, and thermogravimetric and differential scanning calorimetric analysis. SEM images were acquired with a Philips EM 300 scanning electron microscope. Energy-dispersive X-ray analysis was performed on a NORAN Instrument microprobe attached to a JEOL 5410 scanning electron microscope. TEM data were acquired using a JEOL SX100 and a JEOL 2011 transmission electron microscope. HRTEM observations were performed using a JEOL 2000FX microscope at 200 kV. TEM samples were prepared by dispersing the pyrolyzed material onto copper grids in ethanol media and then dried at room temperature. XRD was conducted at room temperature on a Siemens D-5000 diffractometer with $\theta-2\theta$ geometry. XRD data were collected using Cu Kα radiation (40 kV, 30 mA). FTIR measurements were performed on a PerkinElmer FT-IR spectrophotometer model Spectrum BXII.

Photocatalytic Measurements. For the evaluation of the photocatalytic activity of the composites, 30 mL of a buffer solution at pH 7 of 1×10^{-5} M methylene blue (AM) was used. To reduce the adsorption of the dye on the surface, a buffer solution of pH = 7 was used to reach a zero isoelectric point. The same amount of mass (5.6 mg) was added for the composites dissolved in 300 μL of ethanol.

Irradiation was performed with a 300 W xenon lamp model 6258, which presented an incident light intensity of 1250 mW/m^2, measured with a pyranometer. The distance between the lamp and the suspension was 16 cm. The AM concentration

https://doi.org/10.1021/acsomega.0c05811
ACS Omega 2021, 6, 9391−9400

for each sample was determined by UV−vis spectrophotometry. Specifically, the intensity of the maximum absorbance corresponding to the lowest energy peak of the characteristic spectrum of methylene blue at 664 nm was measured. The photocatalytic efficiency of the products is expressed as the variation of the percentage of degradation with respect to the irradiation time.

RESULTS AND DISCUSSION

ThO_2 was prepared by thermal treatment of the chitosan and PVP precursors. The XRD pattern shows the pure phase of ThO_2 arising from these two precursors (see Supporting Information S2), in concordance with the other XRD pattern reported from solution methods.[1,4,5,8,9] SEM images evidence a morphology composed of porous grains of ThO_2 particles arising from both macromolecular complexes (see Figure 1).

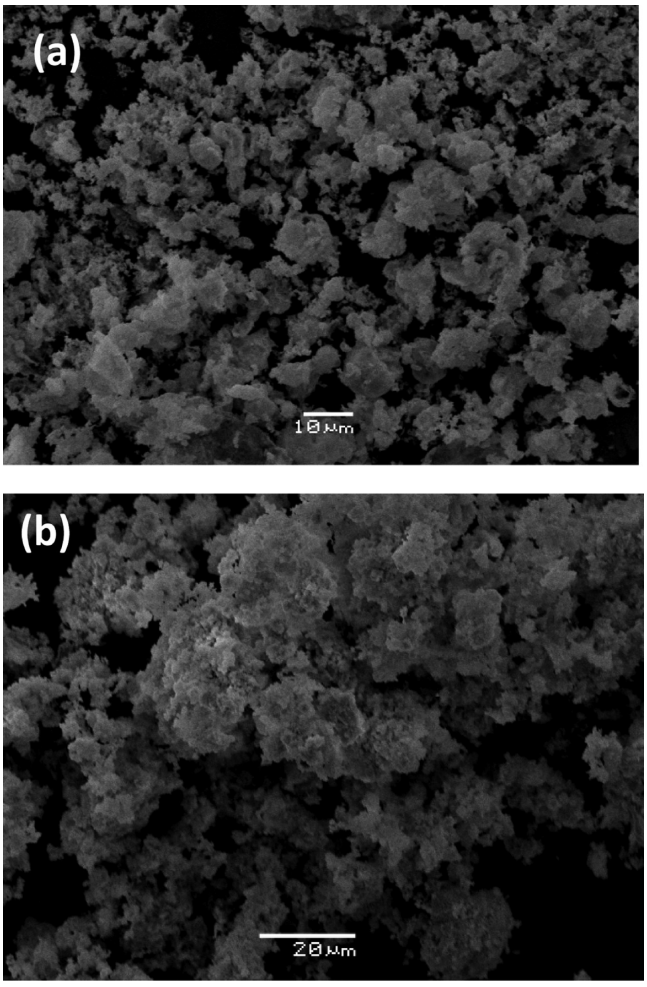

Figure 1. SEM image of ThO_2 from the Chitosan·$Th(NO_3)_4$ precursor (a) and from PS-co-4-PVP·$Th(NO_3)_4$ (b).

Similar morphology was observed for ThO_2 obtained by Moeini et al.,[8] in contrast with more densified grains observed from other solution methods.[4,5] The SEM−EDS analysis for ThO_2 from both precursors shows the expected presence of Th and O (see Supporting Information S3).

TEM images show nanoparticles of average sizes of 50 and 40 nm for ThO_2 from chitosan (Figure 2a) and PVP (Figure 2b) precursors, respectively. Similar particle sizes were observed for ThO_2 obtained by the hydrothermal method.[8]

In Figure 3, HR-TEM images are shown for ThO_2 obtained from the chitosan precursor. Nanoparticles of ThO_2 with sizes of about 10 nm (Figure 3a,b) are observed, which are typically concatenated. Several interplanar distances were indexed, such as 0.32 and 0.28 nm, which correspond to the (111) and (200) interplanar spacings, respectively. Similar results were obtained for the ThO_2 obtained from PVP, as observed in Figure 4a, with a mean size of about 45 nm. An interplanar distance of 0.31 nm corresponding to the (111) interplanar spacing of the ThO_2 was measured (Figure 4d).

In terms of their photoluminescence properties, a very few studies have been reported for ThO_2.[22−26] Our photoluminescence study for the obtained ThO_2 particles is shown in Figure 5. The excitation spectra (not shown), which reveal one broad band at 366 nm, produce an emission wavelength at 697 nm. The position of the band at 366 nm is attributed to absorption of charge transfer $Th^{IV}/Th^{III} \rightarrow Th^{III}/Th^{IV}$ under nonstoichiometric conditions (ThO_{2-X}).[24] The two main emission peaks, around 400 and 420 nm, have been assigned to the Th^{4+} typical center,[22,24] while those at 680 and 710 nm could be ascribed to the formation of oxygen vacancies on the ThO_2 surface, which could be occupied by either oxygen or other impurities.[22,26] Nevertheless, the exact origin of these emissions is not fully clear.[22−26] Additionally, an effect on the emission intensity depending on the nature of the polymer and the metal/polymer ratio of the precursor was also observed (see Figure 5). The ThO_2 prepared from the PVP precursor using a 1:1 metal/polymer ratio exhibits the most intense emission of the maxima peaks at 400 and 420 nm, while that for the PVP precursor using the 1:5 metal/polymer ratio exhibits the most intense emission in the emission at 680 and 710 nm.

Different composites of ThO_2 with SiO_2 were also prepared by pyrolysis at 800 °C under air of the Chitosan·$Th(NO_3)_4$//SiO_2 and PS-co-4-PVP·$Th(NO_3)_4$//SiO_2 precursors. The diffraction pattern of the different obtained products is shown in Supporting Information S4. ThO_2 is weakly observed by XRD due to the dilution of the precursors containing the thorium salts with respect to SiO_2 (1:100), as also previously reported for other metals[27,28] or metal oxides[29] with respect to the amorphous silica. The presence of ThO_2 inside silica was corroborated by SEM−EDS mapping by element analysis. This technique gives also information about the distribution of the thoria into SiO_2. From Figure 6, ThO_2 agglomerated nanoparticles of about 250 nm were observed to be homogeneously dispersed into bigger silica particles. A similar distribution of the ThO_2 nanoparticles, but with bigger sizes of about 950 nm, was observed for ThO_2 inside SiO_2 obtained from the chitosan precursor (Figure 7). The representative SEM image of the ThO_2/SiO_2 composites arising from both macromolecular precursors is displayed in Supporting Information S5. For the ThO_2/chitosan sample, typical nanostructure morphology of that obtained from solid-state pyrolysis can be seen.[13] In some areas, a dense 3D morphology with several shapes joined between them with the presence of pores is exhibited, as shown in Figure S5a,b. On the other hand, sphered shapes were also observed, Figure S5c,d. For ThO_2 from the PS-co-4-PVP·$Th(NO_3)_4$//SiO_2 precursor, big agglomerates composed mainly of spheres of different sizes were observed, see Figure S5a.

XRD patterns of the ThO_2//TiO_2 composites from the chitosan and PVP precursors are shown in Figure S6 of the Supporting Information Again, the TiO_2 matrix presents more

https://doi.org/10.1021/acsomega.0c05811
ACS Omega 2021, 6, 9391−9400

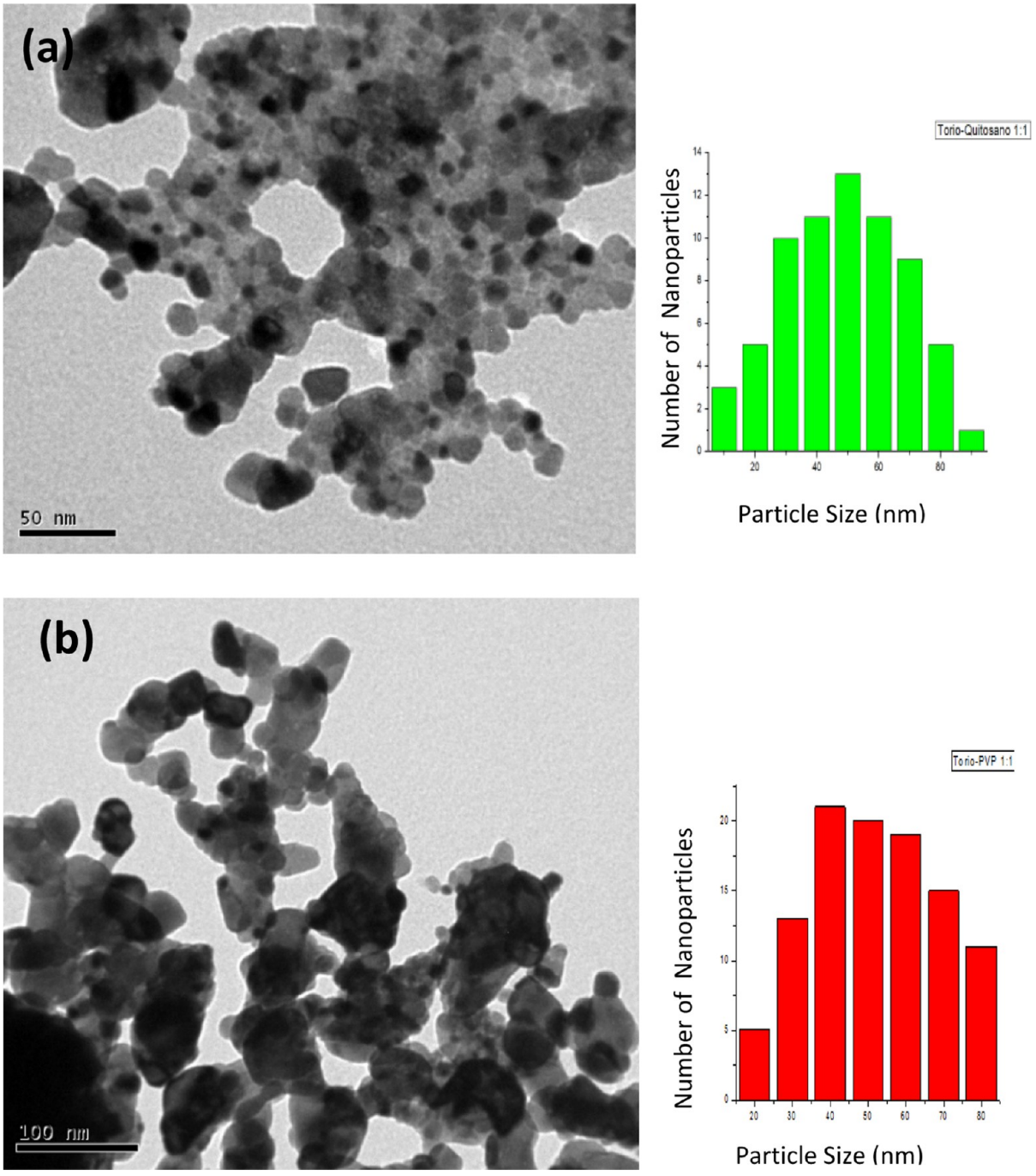

Figure 2. TEM image of ThO_2 from the Chitosan·$Th(NO_3)_4$ precursor (a) and from PS-co-4-PVP·$Th(NO_3)_4$ (b).

intensity than ThO_2, for both cases. Nevertheless, the presence of ThO_2 was clearly identified from the SEM−EDS mapping image (see S7, Supporting Information). Several SEM images of the ThO_2//TiO_2 composite obtained from the chitosan precursor are also shown in Figure 8, where dense grains can be observed. Similar morphology was obtained for ThO_2//TiO_2 composites arising from PVP precursors (see Figure 9).

Finally, SEM−EDS mapping (see Figure S7) exhibits a homogeneous distribution of ThO_2 inside the TiO_2 matrix for ThO_2//TiO_2 composites produced from both precursors.

Photoluminescence of ThO_2/SiO_2 and ThO_2/TiO_2 Composites. In order to investigate the effect of the SiO_2 and TiO_2 matrices on the intensity of ThO_2 particles, the luminescence spectra of ThO_2/SiO_2 and ThO_2/TiO_2 composites were recorded and compared with those of pure ThO_2. The results are plotted in Figure 10.

For the chitosan precursor (Figure 10a), it can be observed that the matrix inclusion produces a decrease in the emission intensity, showing the order ThO_2 > ThO_2/SiO_2 > ThO_2/TiO_2 for both main emissions. In the case of the samples produced from the PVP precursor, Figure 10b, a similar trend was observed for the emission maxima at 680 and 710 nm but an inversion occurs for the emission at 400 and 420 nm, with the order ThO_2 > ThO_2/TiO_2 > ThO_2/SiO_2. These variations of the maxima intensity at 680 and 710 nm could be related with the presence of surface oxygen or impurities generated in the SiO_2 and TiO_2, leading to different morphologies and surface defects induced by these matrices. The detailed

https://doi.org/10.1021/acsomega.0c05811
ACS Omega 2021, 6, 9391−9400

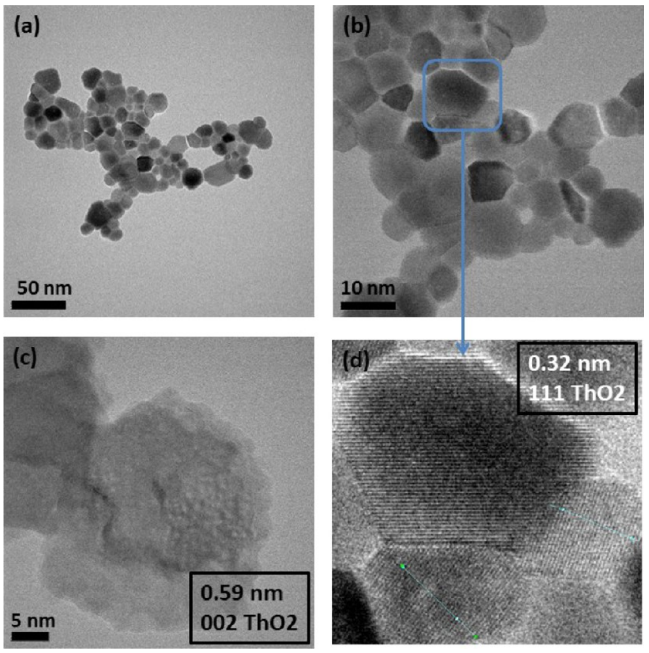

Figure 3. HRTEM image of ThO_2 from Chitosan·$Th(NO_3)_4$ precursors. 50 (a), 10 (b), and 5 μm (c,d).

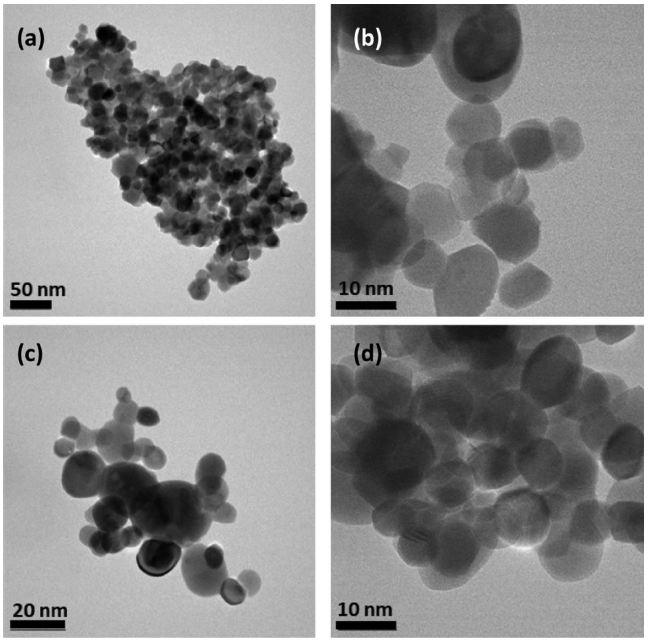

Figure 4. HRTEM image of ThO_2 from PS-co-4-PVP·$Th(NO_3)_4$. 50 (a), 10 (b), 20 (c), and 10 μm (d).

mechanism of how this effect occurs is unknown. In this sense, it was reported that an increase in the emission intensity is normally associated with an increase in the surface defects on the ThO_2 which are occupied by oxygen.[26] As a consequence, according to Figure 10a, the oxygen absorbed on the surface of thoria decreased on the inclusion on SiO_2 and TiO_2. A similar explanation for the observed intensity variation could hold for the ThO_2/PVP sample.

Photocatalytic Activity. Although there are scarce reports about the catalytic activity of thoria, no studies about the photocatalytic activity of ThO_2 neither ThO_2/SiO_2 nor ThO_2/TiO_2 composites toward contaminant dyes have been reported. We have performed studies about the use of thoria acting as a photocatalyst for the degradation of methylene blue under solar radiation. As is shown in Figure 11, thoria exhibited an activity of 66 and 67% in 300 min for ThO_2 prepared form the chitosan and PVP precursors, respectively. The absorption decrease in the absorbance at 655 nm of methylene blue versus wavelength at different time intervals for the different studied samples can be observed in Supporting Information S8. The kinetic degradation of methylene blue with ThO_2/chitosan followed a zero order, while that for ThO_2/PVP followed a first order. Similar kinetic behavior was observed for the ThO_2/SiO_2 and ThO_2/TiO_2 composites, as summarized in Supporting Information S9. On the other hand, the photocatalytic efficiency of the ThO_2/SiO_2 composite decreased to 25 and 28% for the chitosan and PVP precursors, respectively. As for the case of the ThO_2/TiO_2 composite, the photocatalytic efficiency decreased to 39.5 and 27% for the chitosan and PVP precursors, respectively. A summary of the kinetic data is shown in Table 1.

Table 1 shows the obtained values for photodegradation, the speed constant, and the correlation coefficient. In all cases, it is observed that the correlation coefficient (r^2) is close to unity, which indicates that the photocatalytic degradation process, mediated by the synthesized thorium oxides, adjusts to the zero-order and first-order kinetics. The estimated rate constant for the degradation of methylene blue in the presence of thorium prepared without the SiO_2 and TiO_2 matrices is greater than that of the pristine compounds, suggesting that the structural modification and synergy of the inorganic component play a fundamental role. This is related with the increase in the photocatalytic efficiency of the semiconductor, due to the greater number of active sites available by the (ThO_2) *n*-PVP and (ThO_2) *n*-chitosan precursors. The increase in photocatalytic activity of only ThO_2 with respect to the composites ThO_2/SiO_2 and ThO_2/TiO_2 may be due to the greater porosity of thoria alone with respect to the porosity of thoria included in SiO_2 and TiO_2 matrices. This can be observed from the SEM images of only ThO_2, Figure 1, with respect to the SEM images of i ThO_2 included in silica and titania, see Figures 9 and S5 of the Supporting Information. Clearly, the SEM image of ThO_2 is porous, in contrast with the SEM images of ThO_2 including inside SiO_2 and TiO_2 matrices where a dense material is observed.

Band Gap Study. The band gap of metal oxides is an interesting property, which is involved in electronic applications.[30,31] Materials based on thoria are viewed as wide band gap semiconductors. For the case of thoria, there is little information in the literature regarding its band gap. For ThO_2 nanoparticles, Aller et al.[23] reported values in the range 6.22−5.69 eV, while Buono-Core et al.[24] reported values from 4.5 to 4.61 eV for ThO_2 thin films. The study of Aller et al. also reported a wide range of values from 3.84 to 6.9 eV, although some of these values are based on theoretical calculations. Using the solid-state UV−visible absorption and with the Tauc plot for ThO_2, we estimated a value of 5.66 and 5.76 eV for chitosan and PVP precursors, respectively (see Supporting Information S11). These values are in concordance with those previously reported in the literature.[29] For the ThO_2/SiO_2 composite, similar values of 5.50 and 5.60 eV were estimated. In this case, there are no literature data for these composites. On the other hand, the band gap values for thoria included in TiO_2 matrices exhibited values of 3.14 and 3.15 eV for the chitosan and PVP precursors, respectively. These values are

https://doi.org/10.1021/acsomega.0c05811
ACS Omega 2021, 6, 9391−9400

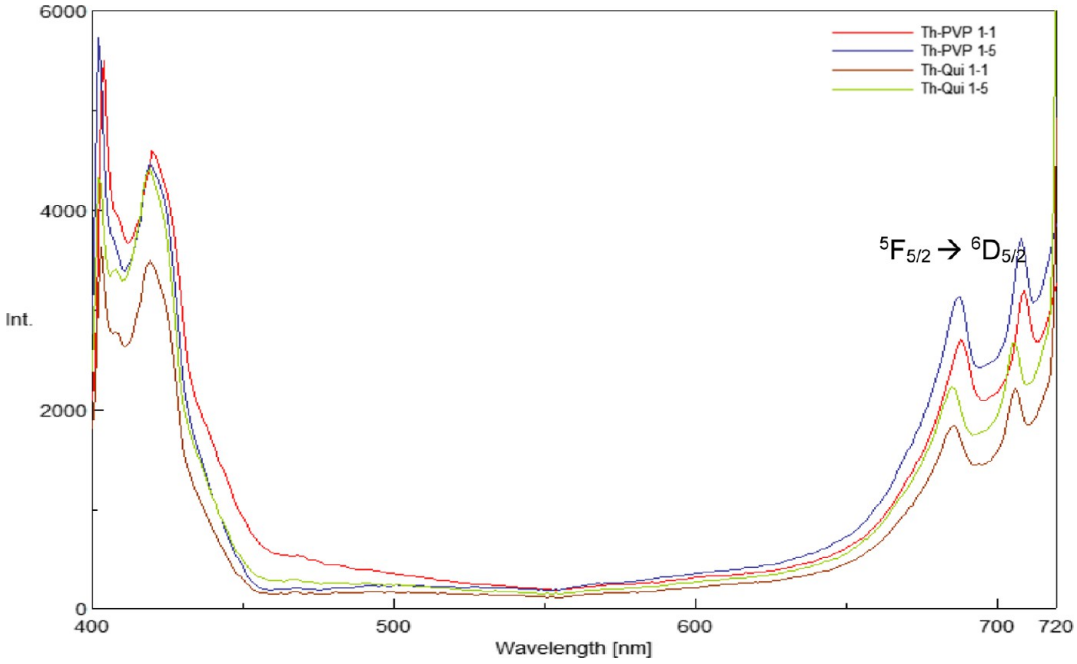

Figure 5. Luminescence spectra of the ThO_2 from the precursors Chitosan·$Th(NO_3)_4$ and PS-co-4-PVP·$Th(NO_3)_4$ in 1:1 and 1:5 molar ratios.

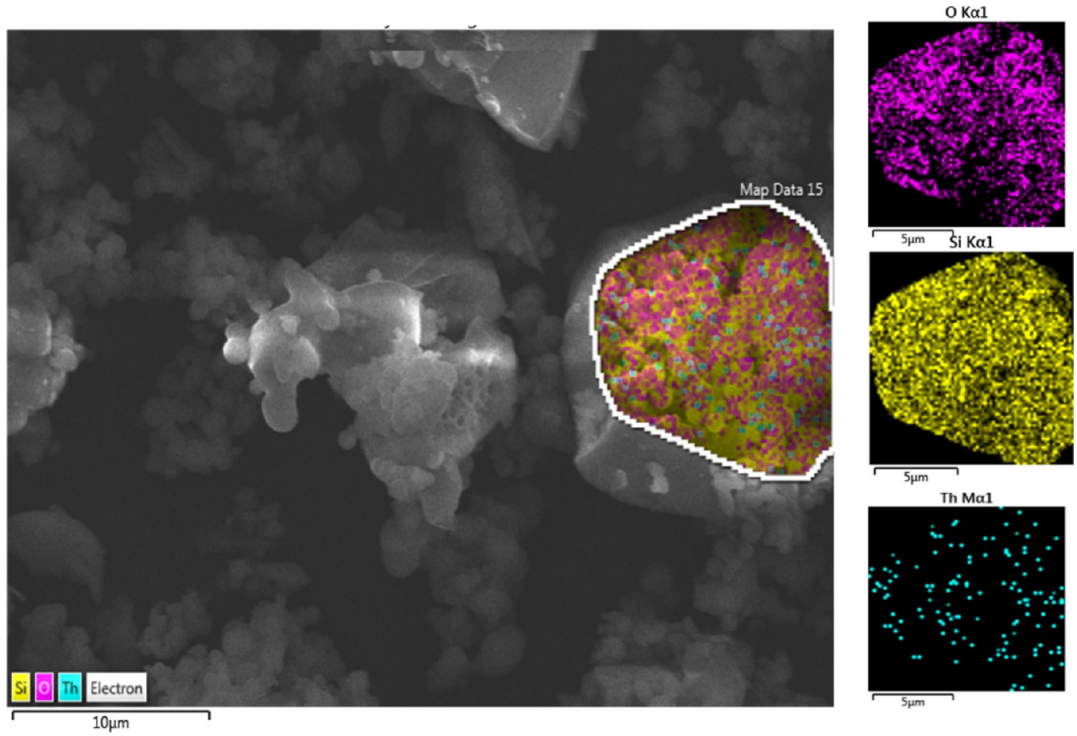

Figure 6. SEM−EDS mapping by elements of ThO_2 inside SiO_2 from the Chitosan·$Th(NO_3)_4$//SiO_2 precursor.

significantly lower than those of ThO_2 and ThO_2/SiO_2. As pointed by Buono-Core et al.,[24] the optical band gap energy is very sensitive to the preparation method and the experimental parameters applied in the synthesis.[24] In fact, Mahmoud also reported a value of 3.82 eV for ThO_2 prepared by a spray pyrolysis technique.[25]

Formation Mechanism Probable. A proposed formation mechanism is discussed here based on previous studies of solid-state nanostructures using the same synthetic approach.[19,32] According to these studies, the first step on heating the samples involves the formation of a 3D network to produce a thermally stable matrix. This step is crucial as it offsets the sublimation (see Figure 12). The first heating step could involve a cross linking of the chitosan or PSP-4-PVP polymer, giving a 3D matrix containing the $Th(NO_3)_4$ compound linked to the polymeric chain. The following steps could involve the organic carbonization, producing holes where the nanoparticles begin to nucleate. As confirmed in earlier studies,[32] the ThO_2 oxide could grow over the layered

https://doi.org/10.1021/acsomega.0c05811
ACS Omega 2021, 6, 9391−9400

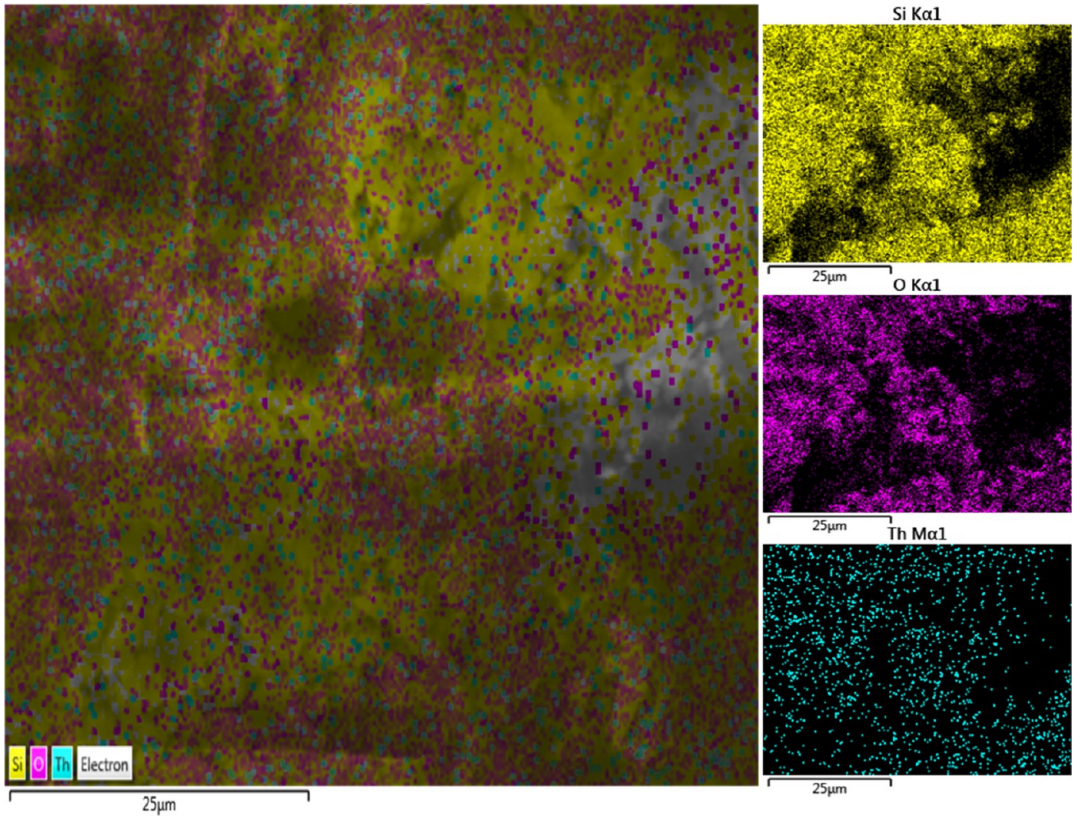

Figure 7. SEM−EDS mapping by elements of ThO_2 inside SiO_2 from the precursor PS-co-4-PVP·$Th(NO_3)_4$//SiO_2.

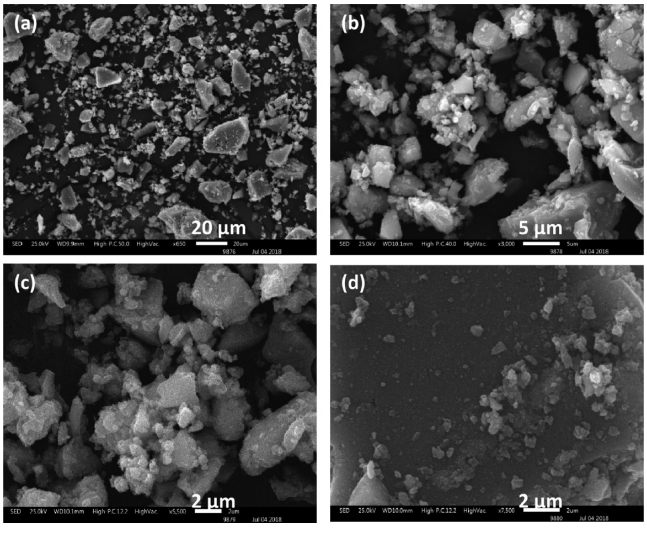

Figure 8. SEM image of the ThO_2//TiO_2 composites arising from the Chitosan·$Th(NO_3)_4$//TiO_2 precursors: 20 (a), 5 (b), and 2 μm (c,d).

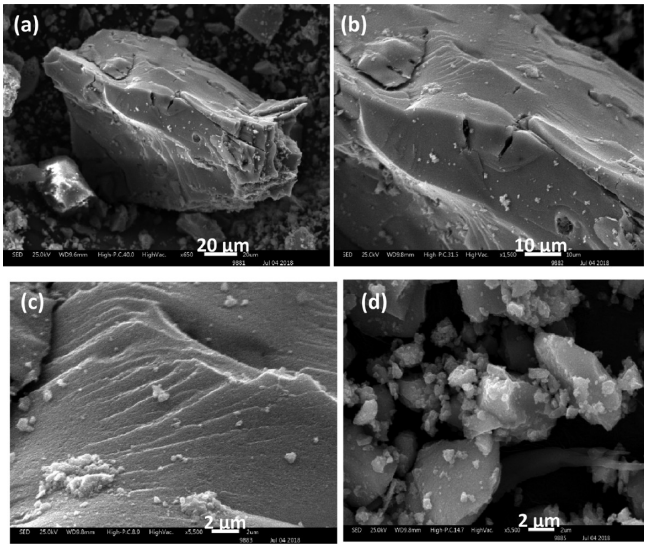

Figure 9. ThO_2//TiO_2 composites arising from the PS-co-4-PVP·$Th(NO_3)_4$//TiO_2 precursors: 20 (a), 10 (b), and 2 μm (c,d).

graphitic carbon host which is lost during the final annealing temperature, that is, 800 °C.

CONCLUSIONS

ThO_2 nanoparticles were satisfactorily prepared by solid-state pyrolysis of the Chitosan·$Th(NO_3)_4$ and PS-co-4-PVP·$Th(NO_3)_4$ precursors. The particle sizes were in the range of 40−50 nm depending on the polymer solid-state template. The luminescence of ThO_2 arising from both polymers exhibits a dependence with the nature of the precursor and with the metal/polymer ratio being the most intense emission for the ThO_2 arising from PS-co-4-PVP·$Th(NO_3)_4$ in the molar ratio 1:1. The photocatalytic efficiency of ThO_2 toward the degradation of methylene blue was around 66% in 300 min for the thoria obtained from both precursors. The inclusion of thoria into the SiO_2 and TiO_2 matrices was achieved by solid-state thermolysis of the solid Chitosan·$Th(NO_3)_4$//MO_2 and PS-co-4-PVP·$Th(NO_3)_4$//MO_2 precursors, where MO_2 = SiO_2 and TiO_2 to give the ThO_2/SiO_2 and ThO_2/TiO_2 composites. SEM−EDS mapping analysis showed a regular dispersion of the thoria into the SiO_2 and TiO_2 matrices. The particle size of

https://doi.org/10.1021/acsomega.0c05811
ACS Omega 2021, 6, 9391−9400

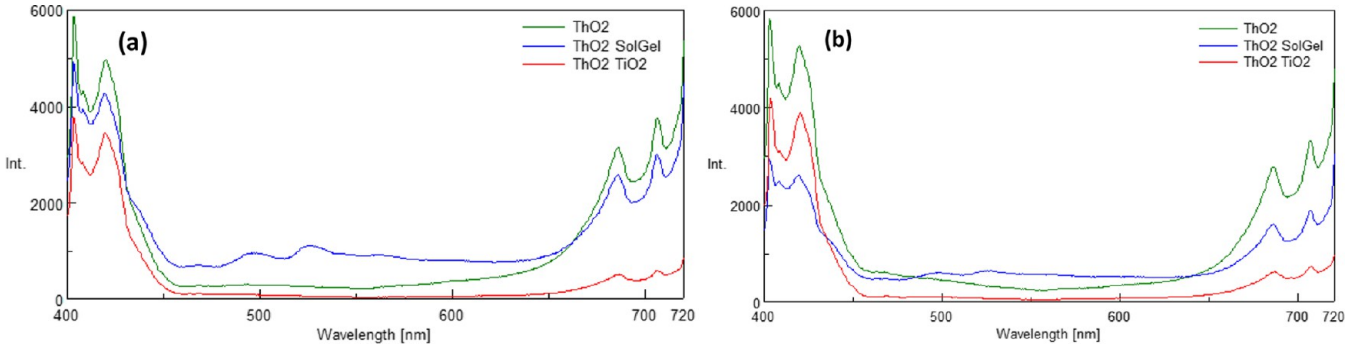

Figure 10. Luminescence spectra of the ThO_2 from the precursors ThO_2, Chitosan·$Th(NO_3)_4$//SiO_2 (a), and PS-co-4-PVP·$Th(NO_3)_4$//TiO_2 (b) $\lambda_{exc.}$ = 366 nm.

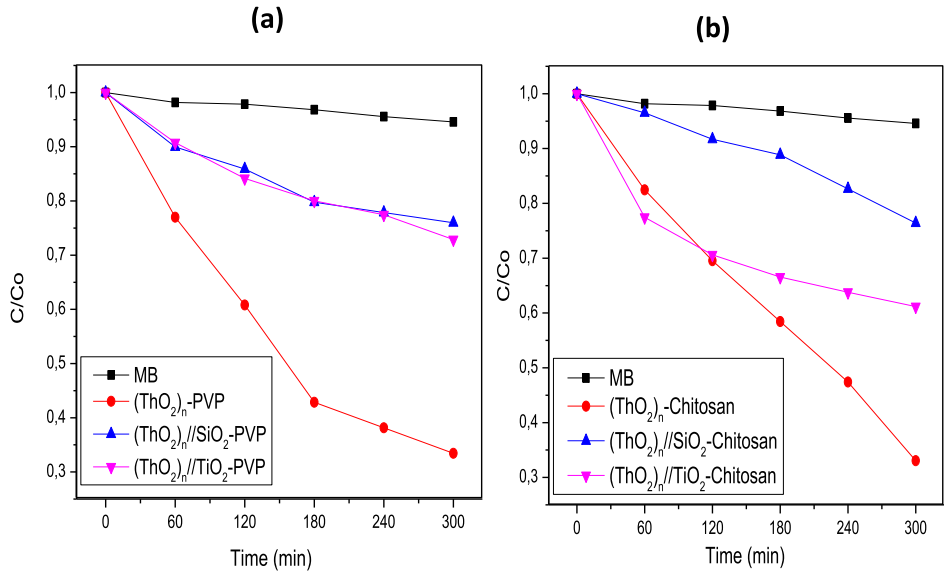

Figure 11. Normalized concentration change in MB without the catalyst and in the presence of ThO_2 from the PS-co-4-PVP·$Th(NO_3)_4$ (a) and Chitosan·$Th(NO_3)_4$ (b) precursors.

Table 1. Kinetic Data for the Photodegradation Process of MB with ThO_2 and with the Composites ThO_2/SiO_2 and ThO_2/TiO_2

photocatalyst	apparent photodegradation	discoloration rate (%)	r^2 linear fit (%)
ThO_2-Chitosan	3.7×10^{-3}	67	0.992
ThO_2-PS-4-PVP	2.2×10^{-3}	66	0.967
ThO_2/SiO_2-Chitosan	7.7×10^{-4}	24	0.979
ThO_2/SiO_2-PS-4-PVP	8.5×10^{-4}	25	0.923
ThO_2/TiO_2-CHITOSAN	1.4×10^{-3}	39	0.815
ThO_2/TiO_2-PS-4-PVP	8.7×10^{-4}	27	0.941

ThO_2 increases by about 19 times for the nanoparticles obtained from chitosan as they are included in SiO_2, while for the ThO_2 obtained from PS-co-4-PVP, an increase of 6 times is observed when the ThO_2/SiO_2 composite is formed. The effect of the polymer precursors on the particle size is little for the free matrices of ThO_2, while that when included inside silica is in the particle size order chitosan > PS-co-4-PVP by nearly four times.

The intensity of the emission at 420 nm followed the order ThO_2 > ThO_2/SiO_2 > ThO_2/TiO_2 which was explained by the surface's defects on the ThO_2 associated with their inclusion into SiO_2 and TiO_2 matrices. The photocatalytic activity

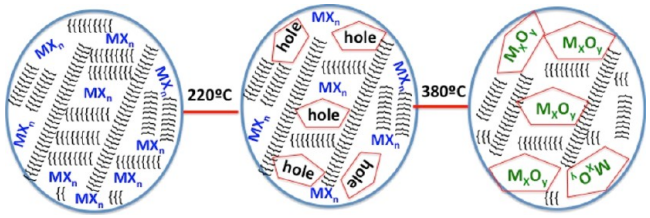

Figure 12. Schematic representation of the proposed mechanism of the formation of the metal oxide nanoparticles. MX_n represents the general formula of the metallic salt coordinated to the chitosan and PSP-4-PVP polymer, $Th(NO_3)_4$ and }}}}}}} represent the chitosan and PSP-4-PVP polymer, respectively. The temperatures are referential general values.

toward methylene blue degradation follows the order of ThO_2 > ThO_2/TiO_2 > ThO_2/SiO_2 and was attributed to the encapsulation of the ThO_2 into the different matrices. Similar results on the effect of the SiO_2, TiO_2, and Al_2O_3 on the nanostructured NiO have recently appeared.[33]

■ ASSOCIATED CONTENT

Supporting Information

The Supporting Information is available free of charge at https://pubs.acs.org/doi/10.1021/acsomega.0c05811.

https://doi.org/10.1021/acsomega.0c05811
ACS Omega 2021, 6, 9391−9400

Experimental details of the synthesis of the precursors; XRD diffraction pattern of ThO_2 from the Chitosan·$Th(NO_3)_4$ and PS-co-4-PVP·$Th(NO_3)_4$ precursors; SEM−EDS image for ThO_2 from precursors Chitosan·$Th(NO_3)$ 1:1 and 1:5 and ThO_2 from the PS-co-4-PVP·$Th(NO_3)_4$ precursor, 1:1 and 1:5; diffraction patterns of Th/SiO_2 from the Chitosan·$Th(NO_3)_4$//SiO_2 precursor and from PS-co-4-PVP·$Th(NO_3)_4$//SiO_2; SEM image from the pyrolytic product of the Chitosan·$Th(NO_3)_4$//SiO_2 precursor at several magnifications; XRD patterns for the ThO_2/TiO_2 composite from the Chitosan·$Th(NO_3)_4$//TiO_2 and PS-co-4-PVP·$Th(NO3)_4$//TiO_2 precursor; SEM−EDS mapping of the composite ThO_2/TiO_2 from the Chitosan·$Th(NO_3)_4$//TiO_2 and PS-co-4-PVP·$Th(NO3)_4$//TiO_2 precursor; decrease absorption of the absorbance at 655 nm of methylene blue versus wavelength at several times for ThO_2, ThO_2/SiO_2, and ThO_2/TiO_2 from the two precursors having PS-co-4-PVP and chitosan polymers; kinetic of the degradation for the ThO_2, ThO_2/SiO_2, and ThO_2/TiO_2 from the two precursors PS-co-4-PVP and chitosan polymers; and Tauc plots for band gap determinations of ThO_2, ThO_2/SiO_2, and ThO_2/TiO_2 (PDF)

AUTHOR INFORMATION

Corresponding Authors

Carlos Diaz − *Departamento de Química, Facultad de Química, Universidad de Chile, Santiago de Chile 7800003, Chile;* orcid.org/0000-0002-4535-4115; Email: cdiaz@uchile.cl

M. L. Valenzuela − *Instituto de Ciencias Químicas Aplicadas, Grupo de Investigación en Energía y Procesos Sustentables, Universidad Autónoma de Chile, Santiago de Chile 8910060, Chile;* orcid.org/0000-0002-5759-2110; Email: maria.valenzuela@uautonoma.cl

Authors

Miguel A. Laguna-Bercero − *Instituto de Nanociencia y Materiales de Aragón (INMA), CSIC-Universidad de Zaragoza, Zaragoza 50009, Spain;* orcid.org/0000-0002-7819-8956

Daniel Carrillo − *Departamento de Química, Facultad de Química, Universidad de Chile, Santiago de Chile 7800003, Chile*

Marjorie Segovia − *Departamento de Química, Facultad de Química, Universidad de Chile, Santiago de Chile 7800003, Chile*

Karina. Mendoza − *Departamento de Química, Facultad de Química, Universidad de Chile, Santiago de Chile 7800003, Chile*

Patricio Cartes − *Departamento de Química, Facultad de Química, Universidad de Chile, Santiago de Chile 7800003, Chile*

Complete contact information is available at: https://pubs.acs.org/10.1021/acsomega.0c05811

Notes

The authors declare no competing financial interest.

ACKNOWLEDGMENTS

The authors acknowledge Fondecyt Projects 1160241 for financial support. This research has also received funding from Consejo Superior de Investigaciones Científicas, Spain under grant I-COOP LIGHT 2015CD0013. The use of Servicio General de Apoyo a las Investigación (SAI, University of Zaragoza) is also acknowledged.

REFERENCES

(1) Lin, Z.-W.; Kuang, Q.; Lian, W.; Jiang, Z.-Y.; Xie, Z.-X.; Huang, R.-B.; Zheng, L.-S. Preparation and Optical Properties of ThO_2 and Eu-Doped ThO_2 Nanotubes by the Sol−Gel Method Combined with Porous Anodic Aluminum Oxide Template. *J. Phys. Chem. B* **2006**, *110*, 23007−23011.

(2) Hudry, D.; Apostolidis, C.; Walter, O.; Gouder, T.; Courtois, E.; Kübel, C.; Meyer, D. Non-aqueous Synthesis of Isotropic and Anisotropic Actinide Oxide Nanocrystals. *Chem.—Eur. J.* **2012**, *18*, 8283−8287.

(3) Hudry, D.; Apostolidis, C.; Walter, O.; Gouder, T.; Courtois, E.; Kübel, C.; Meyer, D. Controlled synthesis of thorium and uranium oxide nanocrystals. *Chem.—Eur. J.* **2013**, *19*, 5297−5305.

(4) Tripathi, V. k.; Nagarajan, R. Sol−Gel Synthesis of High-Purity Actinide Oxide ThO_2 and Its Solid Solutions with Technologically Important Tin and Zinc Ions. *Inorg. Chem.* **2016**, *55*, 12798−12806.

(5) Dash, S.; Singh, A.; Ajikumar, P. K.; Subramanian, H.; Rajalakshmi, M.; Tyagi, A. K.; Arora, A. K.; Narasimhan, S. V.; Raj, B. Synthesis and characterization of nanocrystalline thoria obtained from thermally decomposed thorium carbonate. *J. Nucl. Mater.* **2002**, *303*, 156−168.

(6) Tabakova, T.; Idakiev, V.; Tenchev, K.; Boccuzzi, F.; Manzoli, M.; Chiorino, A. Pure hydrogen production on a new gold−thoria catalyst for fuel cell applications. *Appl. Catal., B* **2006**, *63*, 94−103.

(7) Reibold, R. A.; Poco, J. F.; Baumann, T. F.; Simpson, R. L.; Satcher, J. H. Synthesis and characterization of a nanocrystalline thoria aerogel. *J. Non-Cryst. Solids* **2004**, *341*, 35−39.

(8) Moeini, M.; Malekzadeh, A.; Ahmadi, S. J.; Hosseinpour, M. Synthesis of thoria nanoparticles via the hydrothermal method in supercritical condition. *Mater. Lett.* **2012**, *81*, 99−101.

(9) Wang, L.; Zhao, R.; Wang, X.-W.; Mei, L.; Yuan, L.-Y.; Wang, S.; Chai, Z.-F.; Shi, W.-Q. A facile additive-free method for tunable fabrication of UO_2 and U_3O_8 nanoparticles in aqueous solution. *CrystEngComm* **2014**, *16*, 10469.

(10) Kundrat, V.; Moravec, Z.; Pinkas, J. Preparation of thorium dioxide nanofibers by electrospinning. *J. Nucl. Mater.* **2020**, *534*, 152153.

(11) Plakhova, T. V.; Romanchuk, A. Y.; Likhosherstova, D. V.; Baranchikov, A. E.; Dorovatovskii, P. V.; Svetogorov, R. D.; Shatalova, T. B.; Egorova, T. B.; Trigub, A. L.; Kvashnina, K. O.; Ivanov, V. K.; Kalmykov, S. N. Size Effects in Nanocrystalline Thoria. *J. Phys. Chem. C* **2019**, *123*, 23167−23176.

(12) Verma, S.; Mishra, D.; Sanghi, S. K.; Srivastava, A. K.; Amritphale, S. S. An Instant, Green, Microwave Irradiated Process for the Preparation of Advanced, Hybrid, Nanoflower of Thorium Oxide and Thorium Oxalate Hydrate Useful for Broad Application Spectrum. *Prot. Met. Phys. Chem. Surf.* **2019**, *55*, 65−71.

(13) Díaz, C.; Valenzuela, M. L. In *"Metallic Nanostructures Using Oligo and Polyphosphazenes as Template or Stabilizer in Solid State" in Encyclopedia of Nanoscience and Nanotechnology*; Nalwa, H. S., Ed.; American Scientific Publishers, 2010; Vol. *16*, pp 239−256.

(14) Pileni, M.-P. Self-Assembly of Inorganic Nanocrystals: Fabrication and Collective Intrinsic Properties. *Acc. Chem. Res.* **2007**, *40*, 685−693.

(15) Pileni, M. P. 2D superlattices and 3D supracrystals of metal nanocrystals: a new scientific adventure. *J. Mater. Chem.* **2011**, *21*, 16748−16758.

(16) Wan, Y. F.; Goubet, N.; Albouy, P. A.; Pileni, M. P. Hierarchy in Au Nanocrystal Ordering in Supracrystals: A Potential Approach to Detect New Physical Properties. *Langmuir* **2013**, *29*, 7456−7463.

(17) Ray, C.; Pal, T. Retracted Article: Recent advances of metal−metal oxide nanocomposites and their tailored nanostructures in

numerous catalytic applications. *J. Mater. Chem. A* **2017**, *5*, 9465−9487.
(18) Liu, S.; Han, M.-Y. Silica-Coated Metal Nanoparticles. *Chem.−Asian J.* **2010**, *5*, 36−45.
(19) Díaz, C.; Valenzuela, M. L.; Laguna-Bercero, M. A.; Orera, A.; Bobadilla, D.; Abarca, S.; Peña, O. Synthesis and magnetic properties of nanostructured metallic Co, Mn and Ni oxide materials obtained from solid-state metal-macromolecular complex precursors. *RSC Adv.* **2017**, *7*, 27729−27736.
(20) Díaz, C.; Barrientos, L.; Carrillo, D.; Valdebenito, J.; Valenzuela, M. L.; Allende, P.; Geaneye, H.; O'Dwyer, C. Solventless method for efficient photocatalytic α-Fe 2 O 3 nanoparticles using macromolecular polymeric precursors. *New J. Chem.* **2016**, *40*, 6768.
(21) Díaz, C.; Valenzuela, M. L.; Segovia, M.; Correa, K.; de la Campa, R.; Presa Soto, A. Solution, Solid-State Two Step Synthesis and Optical Properties of ZnO and SnO_2 Nanoparticles and Their Nanocomposites with SiO2. *J. Cluster Sci.* **2018**, *29*, 251−266.
(22) Brysse, M.; Clude, B.; Faure, L.; Guerin, M. Role of surface and bulk impurities in the adsorboluminescence and photoluminescence of thorium dioxide. *J. Lumin.* **1979**, *18*, 402−406.
(23) Pereira, F. J.; Castro, M. A.; Vázquez, M. D.; Debán, L.; Aller, A. J. Optical properties of ThO2−based nanoparticles. *J. Lumin.* **2017**, *184*, 169−178.
(24) Huentupil, Y.; Cabello-Guzmán, G.; Chornik, B.; Arancibia, R.; Buono-Core, G. E. Photochemical deposition, characterization and optical properties of thin films of ThO_2. *Polyhedron* **2019**, *157*, 225−231.
(25) Mahmoud, S. A. Characterization of thorium dioxide thin films prepared by the spray pyrolysis technique. *Solid State Sci.* **2002**, *4*, 221−228.
(26) Hubert, S.; Simoni, E. Luminescence and photoconductivity of pure β-ThBr4 single crystal. *J. Lumin.* **1988**, *40*−*41*, 349−350.
(27) Han, J.; Fang, P.; Jiang, W.; Li, L.; Guo, R. Ag-Nanoparticle-Loaded Mesoporous Silica: Spontaneous Formation of Ag Nanoparticles and Mesoporous Silica SBA-15 by a One-Pot Strategy and Their Catalytic Applications. *Langmuir* **2012**, *28*, 4768−4775.
(28) Thomas, S.; Nair, S. K.; Jamal, E. M. A.; Al-Harthi, S. H.; Varma, M. R.; Anantharaman, M. R. Size-dependent surface plasmon resonance in silver silica nanocomposites. *Nanotechnology* **2008**, *19*, 075710.
(29) Kuwahara, Y.; Furuichi, N.; Seki, H.; Yamashita, H. One-pot synthesis of molybdenum oxide nanoparticles encapsulated in hollow silica spheres: an efficient and reusable catalyst for epoxidation of olefins. *J. Mater. Chem. A* **2017**, *5*, 18518−18526.
(30) Srivastava, A. K. *Oxide Nanostructures*; Pan Stanford: Danver, 2014.
(31) Guo, Y.; Ma, L.; Mao, K.; Ju, M.; Bai, Y.; Zhao, J.; Zeng, X. C. Eighteen functional monolayer metal oxides: wide bandgap semiconductors with superior oxidation resistance and ultrahigh carrier mobility. *Nanoscale Horiz.* **2019**, *4*, 592.
(32) Díaz, C.; Valenzuela, M. L.; Lavayen, V.; O'Dwyer, C. Layered graphitic carbon host formation during liquid-free solid state growth of metal pyrophosphates. *Inorg. Chem.* **2012**, *51*, 6228−6236.
(33) Díaz, C.; Valenzuela, M. L.; Cifuentes-Vaca, O.; Segovia, M.; Laguna-Bercero, M. A. Incorporation of NiO into SiO_2, TiO_2, Al_2O_3, and $Na_{4.2}Ca_{2.8}(Si_6O_{18})$ Matrices: Medium Effect on the Optical Properties and Catalytic Degradation of Methylene Blue. *Nanomaterials* **2020**, *10*, 2470.

https://doi.org/10.1021/acsomega.0c05811
ACS Omega 2021, 6, 9391−9400